

## Article

# Reaction Behavior and Formation Mechanism of $ZrB_2$ and $ZrC$ from the Ni-Zr- $B_4C$ System during Self-Propagating High-Temperature Synthesis

Jiaying Xu <sup>1,\*</sup>, Pengfei Ma <sup>1,\*</sup>, Binglin Zou <sup>2</sup> and Xue Yang <sup>1</sup><sup>1</sup> College of Science, Jilin Institute of Chemical Technology, Jilin 132022, China<sup>2</sup> State Key Laboratory of Rare Earth Resources Utilization, Changchun Institute of Applied Chemistry, Chinese Academy of Sciences, Changchun 130022, China

\* Correspondence: xujiaying@jlicet.edu.cn (J.X.); mapf@jlicet.edu.cn (P.M.); Tel.: +86-187-44220760 (J.X.)

**Abstract:** Self-propagating high-temperature synthesis (SHS) is a good way to prepare  $ZrB_2$ - $ZrC$ /metal cermet composites. In this work,  $ZrB_2$ - $ZrC$ /Ni cermet composites with various Ni contents were successfully fabricated by SHS using the Ni-Zr- $B_4C$  system. The effects of Ni content and particle size of the  $B_4C$  powder on the SHS reaction were investigated. The results indicated that with an increase in Ni content, the adiabatic temperature, maximum combustion temperature, ignition delay time, and ceramic particle size in the product all showed a gradually decreasing trend. The SHS products and the ignition of the SHS reactions were significantly dependent on the  $B_4C$  particle size. The formation mechanism of  $ZrB_2$  and  $ZrC$  during SHS from the Ni-Zr- $B_4C$  system was proposed based on the combustion wave quenching experiment.

**Keywords:** self-propagating high-temperature synthesis (SHS);  $ZrB_2$ ;  $ZrC$ ; reaction behavior; formation mechanism



**Citation:** Xu, J.; Ma, P.; Zou, B.; Yang, X. Reaction Behavior and Formation Mechanism of  $ZrB_2$  and  $ZrC$  from the Ni-Zr- $B_4C$  System during Self-Propagating High-Temperature Synthesis. *Materials* **2023**, *16*, 354. <https://doi.org/10.3390/ma16010354>

Academic Editor: A. Javier Sanchez-Herencia

Received: 15 November 2022

Revised: 15 December 2022

Accepted: 28 December 2022

Published: 30 December 2022



**Copyright:** © 2022 by the authors. Licensee MDPI, Basel, Switzerland. This article is an open access article distributed under the terms and conditions of the Creative Commons Attribution (CC BY) license (<https://creativecommons.org/licenses/by/4.0/>).

## 1. Introduction

Particle reinforced metal matrix composites have attracted increasing attention because of their excellent performance.  $ZrB_2$  and  $ZrC$  have high hardness, a high melting point, good corrosion resistance, and excellent thermodynamic stability, and also exhibit outstanding compatibility with the metal matrix, making them ideal materials for particle reinforcement phases [1–5].

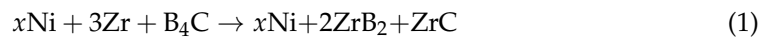
Self-propagating high temperature synthesis (SHS) is a good way to prepare particle reinforced metal matrix composites because of its numerous advantages, such as a rapid synthesis of materials, low energy consumption, and high product purity [6–12]. In recent years, it has been reported that  $ZrC$ - $ZrB_2$ /metal cermets were prepared by adding different metal elements into the Zr- $B_4C$  system and using metal-Zr- $B_4C$  as reaction system, and the reaction mechanism was investigated. Hu Qiaodan et al. [1] prepared  $ZrC$ - $ZrB_2$ /Al and studied the SHS reaction mechanism of the Al-Zr- $B_4C$  system, pointing out that Al plays a very important role in the Al-Zr- $B_4C$  system. At first, molten Al reacted with Zr, and then  $ZrAl_3$  formed the Al-Zr liquid phase, which provided a way for B and C atoms to enter the liquid phase, and finally,  $ZrC$  and  $ZrB_2$  precipitated out of the liquid. Zhang Mengxian et al. [4,5] studied the formation path of  $ZrB_2$  and  $ZrC$  in the Cu-Zr- $B_4C$  system during SHS using a differential scanning calorimeter (DSC) and X-ray diffraction (XRD). The effects of Cu content,  $B_4C$  particle size, and heating rate on the SHS reaction behavior were also studied. Zhang Mengxian et al. [2,3] also studied the reaction behavior in the Co-Zr- $B_4C$  system during SHS. The  $ZrC$ - $ZrB_2$  ceramic composite powders were in situ synthesized by SHS using the Co-Zr- $B_4C$  system, and then plasma was sprayed to form cermet coatings on an Mg alloy. The addition of metal can increase the contact area of the reactants by forming an intermediate liquid phase, thus reducing the difficulty of the reaction. Ni is a promising

candidate, with a low wetting angle with the ceramic phases, and Ni can react with  $B_4C$  to form an Ni-B liquid phase [7,9].

In our previous paper [13], ZrC-ZrB<sub>2</sub>/Ni cermet powders were successfully synthesized by SHS using an Ni-Zr-B<sub>4</sub>C system. The SHS-derived powders were deposited on an Mg alloy to form ZrC-ZrB<sub>2</sub>/Ni cermet coatings by using atmospheric plasma spraying. The produced coatings bonded well with the substrate and provided superior wear resistance. In another previous paper [14], the reaction mechanism in an Ni-Zr-B<sub>4</sub>C system to form ZrB<sub>2</sub>, and ZrC was analyzed by DSC and XRD. In general, DSC experimental conditions are slightly different from SHS reaction conditions in a glove box. Therefore, in this work, the combustion wave quenching experiment was used to reveal the SHS reaction mechanism in a glove box, and the effects of Ni content and different B<sub>4</sub>C reactants on the system products were studied. This is expected to provide a theoretical basis and guidance for the SHS of cermet composites.

## 2. Materials and Methods

The ZrB<sub>2</sub>-ZrC/Ni cermet composites were synthesized according to the following reaction equation:



Commercial Ni ( $\leq 48 \mu\text{m}$ , 99% purity, ST-nano science and technology Ltd. Co., Shanghai, China), Zr ( $\leq 38 \mu\text{m}$ , 99% purity, ST-nano science and technology Ltd. Co., Shanghai, China), and B<sub>4</sub>C ( $\leq 3.5 \mu\text{m}$ ;  $\leq 14 \mu\text{m}$ ;  $\leq 28 \mu\text{m}$ ;  $\leq 40 \mu\text{m}$ ,  $\leq 80 \mu\text{m}$ , 95% purity, Abrasive Ltd. Co., Dunhua, China) powders were used as the starting materials. When studying the influence of Ni content on the SHS reaction, the particle size of B<sub>4</sub>C was selected as 3.5  $\mu\text{m}$ . The particle size of the B<sub>4</sub>C powders varied from 3.5  $\mu\text{m}$  to 80  $\mu\text{m}$  to investigate the effect of the reactant particle size. The Zr and B<sub>4</sub>C powders, with a ratio corresponding to that of stoichiometric 2ZrB<sub>2</sub>-ZrC (mole ratio) mixed with 0–50 wt.% Ni content, were selected for the powder blends. The raw reactant powders were dry-mixed by ball milling at a low speed ( $\sim 50 \text{ rpm}$ ) for 6 h, and then pressed into cylindrical compacts (about 20 mm in diameter and  $15 \pm 2 \text{ mm}$  in height) using a stainless steel die to acquire densities of  $60 \pm 2\%$  theoretical density. The SHS reaction was performed in a self-made glove box filled with argon gas at 0.1 MPa. The green compact was placed on a thin graphite flake and subsequently ignited from the bottom by an arc welding flame with a strong current of 60 A. A small hole with a radius of 2 mm and a depth of 2 mm was drilled at the top of the compact. A pair of W-5% Re/W-26% Re thermocouples was inserted into the hole and linked up with an temperature acquisition recorder to obtain a time–temperature curve. The acquisition speed was 20 points per second. The schematic diagram of the SHS experimental apparatus is shown in Figure 1.

The phase composition of the SHS products was analyzed using an X-ray diffractometer (XRD) (D8 Advance, Bruker, Cu-K $\alpha$  radiation,  $\lambda = 0.15406 \text{ nm}$ , Germany) at a scanning rate of  $6^\circ/\text{min}$  and a scanning range of  $20\text{--}80^\circ$ . The microstructure of the SHS products was examined by scanning electron microscopy (SEM) (S-4800, Hitachi, Tokyo, Japan) equipped with energy dispersive spectroscopy (EDS). The linear intersection of the SEM image was used to measure the size of the ceramic particles.

The combustion wave quenching experiment is a good method to use for studying the reaction mechanism of SHS. The copper-mold-aided combustion wave quenching experiment, using the Ni-Zr-B<sub>4</sub>C system with 30 wt.% Ni in the compact, was performed. The particle size of B<sub>4</sub>C in the quenching experiment was 14  $\mu\text{m}$ . Figure 2 shows the schematic diagram of the combustion wave quenching experimental device. When the combustion wave passed through a rectangular bar 65 mm  $\times$  10 mm  $\times$  5 mm in size, the heat loss increased due to the elongated shape of the bar and the cooling of two copper plates clamped in the middle of the bar, thus achieving the automatic flow blocking of the combustion wave. The quenched bar was carefully polished. The phase composition of the different regions of the SHS quenched bar was identified by X-ray micro-diffraction (D8 Discover with GADDS, Bruker AXS, Karlsruhe, Germany), which was operated at

40 kV and 30 mA using an 800  $\mu\text{m}$  beam diameter. The microstructure of the Ni, Zr,  $\text{B}_4\text{C}$  raw material powder and the different regions of the quenched bar were observed by SEM (S-4800, Hitachi, Japan), respectively. Element distribution at the combustion region was analyzed by EDS.

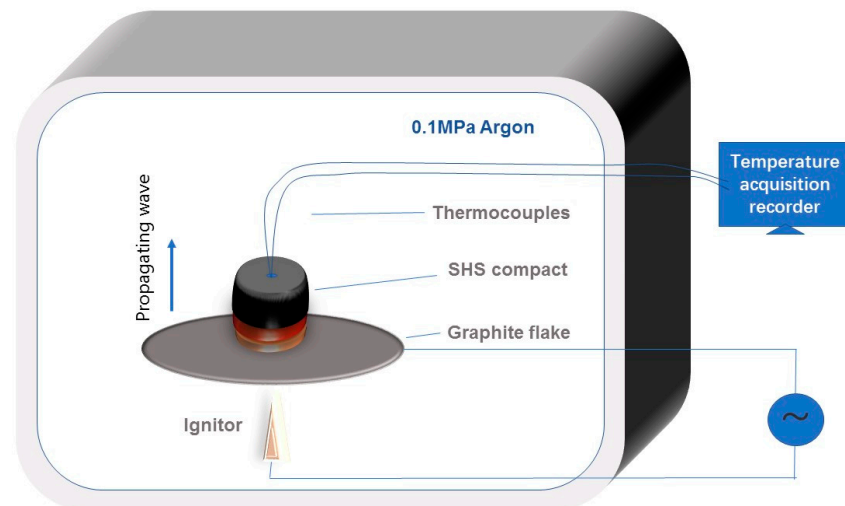


**Figure 1.** The schematic diagram of the SHS experimental apparatus.

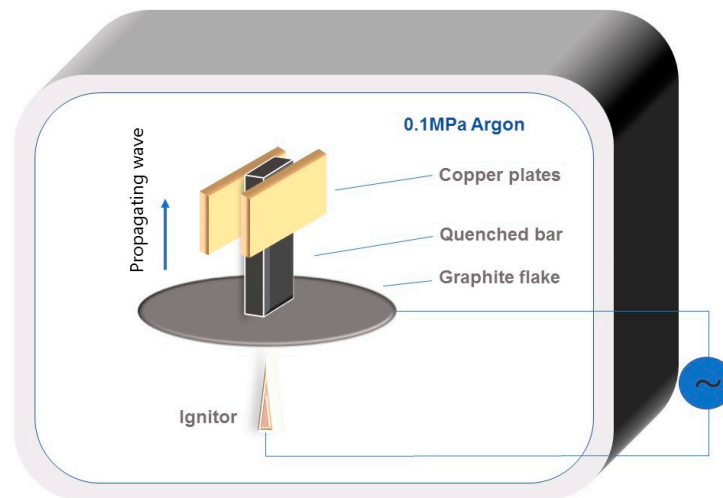


**Figure 2.** The schematic diagram of the combustion wave quenching experimental device.

### 3. Results and Discussion

#### 3.1. Reaction Behavior of the Ni-Zr- $\text{B}_4\text{C}$ System

##### 3.1.1. Effect of Ni Content on the SHS Reaction

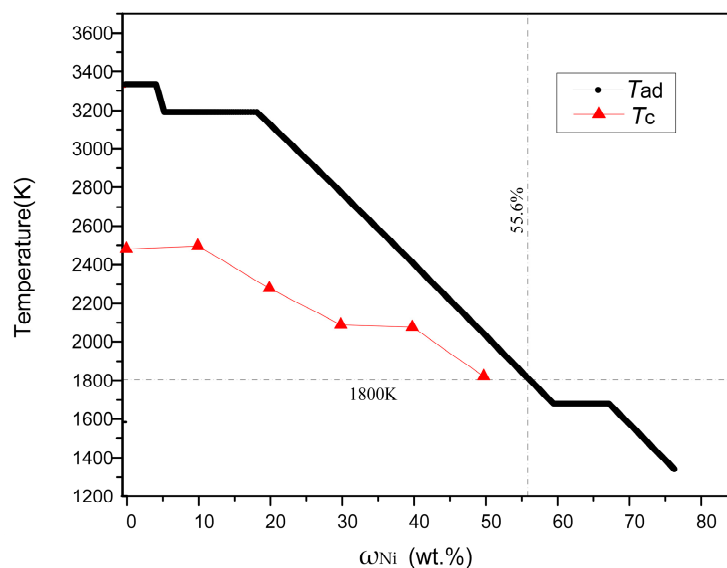
The use of heat generated by the exothermic reaction itself for material synthesis is one of the most basic characteristics of SHS technology [8]. Therefore, thermodynamic analysis of the combustion system is the basis of studying the SHS process. The adiabatic temperature ( $T_{\text{ad}}$ ) is one of the most important thermodynamic parameters to describe the SHS reaction, which can be defined as the theoretically calculated temperature under an adiabatic condition during the SHS process. It can not only be used as a qualitative basis to judge whether the combustion reaction is self-propagating, but it can also predict the state of the combustion reaction products and provide a foundation for the composition design of the reaction system. Merzhanov et al. [15] proposed an empirical criterion such that when  $T_{\text{ad}} \geq 1800$  K, the SHS reaction can be self-propagating.  $T_{\text{ad}}$  can be calculated by computer

programming using thermodynamic data from Ref. [16], according to Equation (2), as follows [15]

$$\Delta H(298) + \int_{298}^{T_{ad}(298)} \sum n_j C_p(P_j) dT + \sum_{298-T_{ad}(298)} n_j L(P_j) = 0 \quad (2)$$

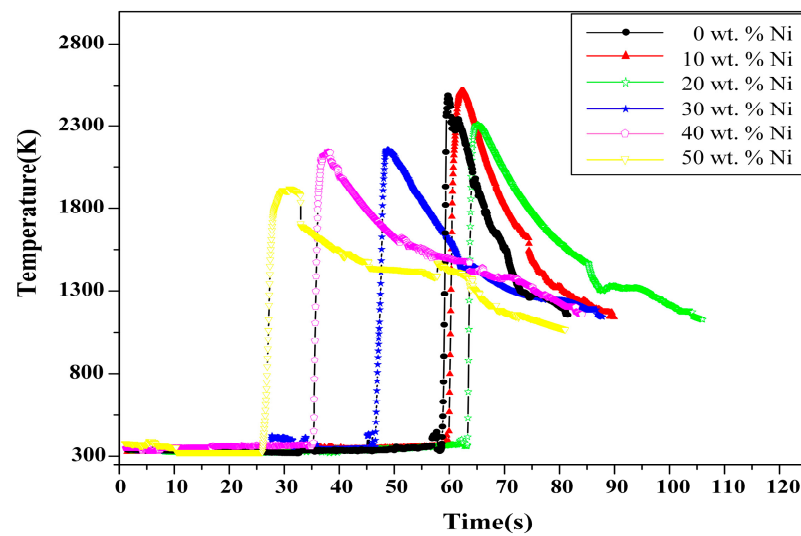
where  $\Delta H(298)$  is the reaction enthalpy at 298 K,  $C_p(P_j)$  and  $L(P_j)$  are the heat capacity and latent heat of the products (if a phase change takes place), and  $P_j$  and  $n_j$  refer to the products and the stoichiometric constant, respectively.

The variation in  $T_{ad}$  with Ni content ( $\omega_{Ni}$ ) is shown in Figure 3. When  $\omega_{Ni}$  is between 0–4 wt.%, 5.23–17.66 wt.% and 57.62–65.04 wt.%, respectively, three temperature platforms appear in the figure. The temperatures are 3323 K, 3187 K, and 1726 K, corresponding to the melting point of  $ZrB_2$ , the boiling point of Ni, and the melting point of Ni, respectively. In these three platform ranges, the  $T_{ad}$  remains constant as the Ni content changes. This is because materials need to absorb a certain amount of heat during phase changes such as melting and gasification. Outside the three platforms, the  $T_{ad}$  decreases with the increase in Ni content. This is due to the increase in Ni content, which leads to a decrease in the amount of Zr and  $B_4C$ , and a decrease in the heat released from the reaction. As shown in Figure 3, when the  $\omega_{Ni}$  is 55.6 wt.%, the calculated  $T_{ad}$  is 1800 K. According to the empirical criterion, when  $T_{ad} \geq 1800$  K, the combustion reaction can be self-sustained [15]. Therefore, the range of  $0\% \leq \omega_{Ni} \leq 50\%$  was selected in this work. The SHS reactions of the Ni-Zr- $B_4C$  system with  $\omega_{Ni} = 0, 10, 20, 30, 40,$  and  $50$  wt.% were all successfully ignited and self-propagated, which was consistent with the theoretical prediction.



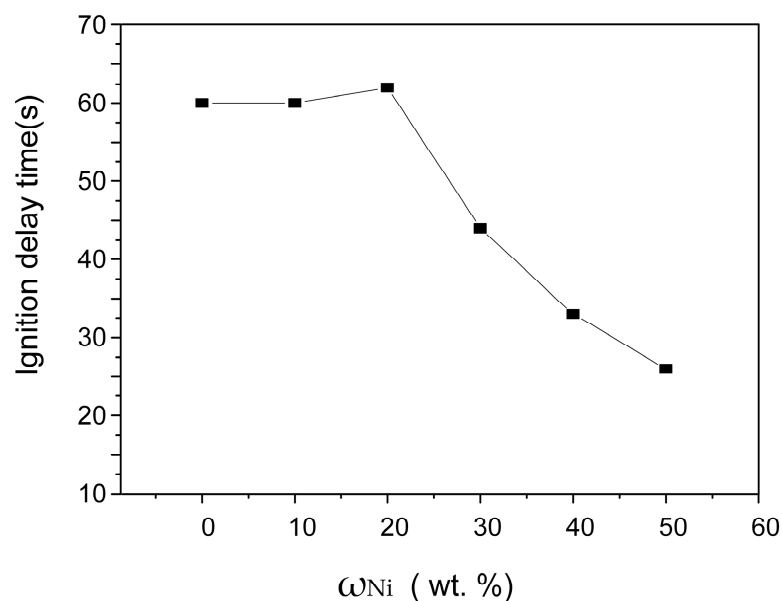
**Figure 3.** Variation in the  $T_{ad}$  and  $T_c$  of the Ni-Zr- $B_4C$  system with various Ni contents.

Figure 4 shows the SHS combustion time–temperature curves of the reactant compacts with various Ni contents in the Ni-Zr- $B_4C$  system. According to the curves, the maximum combustion temperature ( $T_c$ ) decreases with the increase in Ni content. The  $T_c$  of each content was plotted as a curve and compared with  $T_{ad}$ , as observed in Figure 3. It is revealed that the value of  $T_c$  is smaller than that of the corresponding  $T_{ad}$  due to heat loss and incomplete conversion in the actual SHS experiment [3,9]. Moreover, with the increase in Ni content, the difference between  $T_c$  and  $T_{ad}$  decreases gradually. It is worth mentioning that the type of time–temperature curve (yellow curve) changes when 50% Ni is added. At the peak of the curve, the temperature drops more slowly, and temperature peak smoothing is observed. It is presumed that in this case, the exothermic reactions of the formation of the final product are less intense than in other systems [17–19]. With the increase in Ni content, the heat release decreases gradually.



**Figure 4.** Time–temperature curves of the reactant compacts with various Ni contents during the SHS process.

The influence of Ni content on the SHS reaction ignition delay ( $t_{ig}$ ) can also be obtained from the combustion temperature measurement results of samples with different Ni content, as illustrated in Figure 5. With the Ni content increasing,  $t_{ig}$  shows a decreasing trend. Therefore, adding an appropriate amount of Ni to the Zr-B<sub>4</sub>C system can promote the ignition reaction. Previous investigations [14] have studied the formation path of ZrB<sub>2</sub> and ZrC ceramic particles in the Ni-Zr-B<sub>4</sub>C system under DSC conditions, pointing out that initially, Ni reacts with B<sub>4</sub>C and Zr, which can form Ni-B and Ni-Zr melt in the subsequent heating process. The liquid melt is tightly wrapped with B<sub>4</sub>C. It provides a convenient way for B and C atoms to dissolve into the liquid phase, so that the Ni-Zr-B-C quaternary liquid phase can be easily formed, which accelerates the reaction precipitation of ZrB<sub>2</sub> and ZrC. Therefore, the addition of Ni makes the SHS reaction easier to ignite [3].



**Figure 5.** Variation in the ignition delay time ( $t_{ig}$ ) with various Ni contents.

Figure 6 shows the XRD patterns for the products in the Ni-Zr-B<sub>4</sub>C system with different reactant Ni contents. The phase composition of the SHS products with 0 wt.% Ni consists of ZrB<sub>2</sub> and ZrC. When  $\omega_{Ni} = 10\text{--}30$  wt.%, the combustion synthesis products

contain a small amount of  $\text{Ni}_2\text{B}$  in addition to Ni,  $\text{ZrB}_2$ , and  $\text{ZrC}$ . When  $\omega_{\text{Ni}} = 40\text{--}50$  wt.%, the intermediate phases  $\text{Ni}_{10}\text{Zr}_7$  and  $\text{Ni}_4\text{B}_3$  appear and increase with the increase in Ni content, while  $\text{Ni}_2\text{B}$  decrease with the increase in Ni content. This indicates that when the Ni content is greater than 40 wt.%, the incomplete degree of SHS reaction gradually increases, and too much Ni blocks the reaction of Zr and  $\text{B}_4\text{C}$ . In addition, it can also be noted in the figure that when the Ni content is low, the peak intensity of  $\text{ZrB}_2$  is higher than that of  $\text{ZrC}$ , but with the increase in Ni content, the peak intensity of  $\text{ZrB}_2$  gradually becomes weaker than that of  $\text{ZrC}$ . This occurs because with the increase in Ni content, the reaction heat release of the system decreases, and the degree of incomplete reaction increases. A large amount of intermediate  $\text{Ni}_2\text{B}$  has not yet participated in the reaction to form  $\text{ZrB}_2$ .

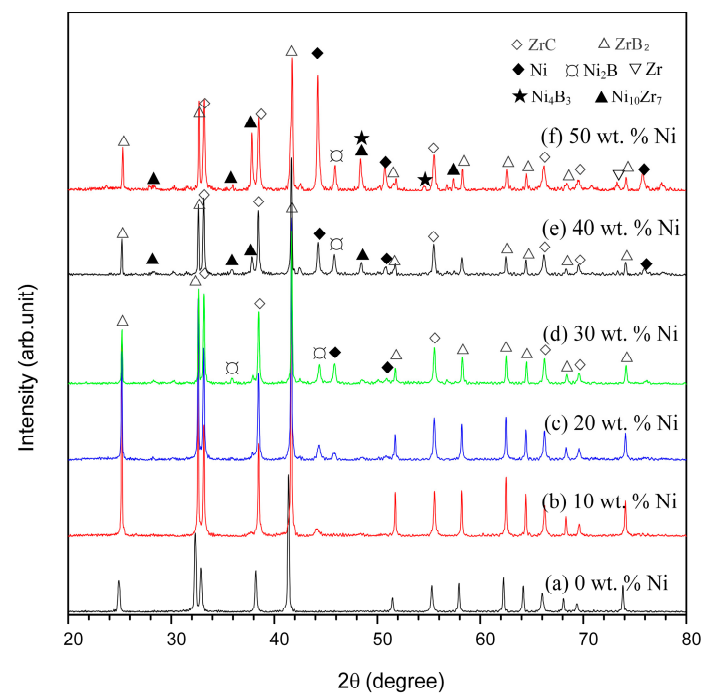


**Figure 6.** XRD patterns for the SHS products with different reactant Ni contents in Ni-Zr- $\text{B}_4\text{C}$  system: (a) 0 wt.%, (b) 10 wt.%, (c) 20 wt.%, (d) 30 wt.%, (e) 40 wt.%, and (f) 50 wt.%.

Figure 7 exhibits the microstructures of the SHS products with different Ni contents. It can be seen that granular  $\text{ZrB}_2$  and  $\text{ZrC}$  are formed in the product. The flat hexagonal particles are  $\text{ZrB}_2$ , and the cube particles are  $\text{ZrC}$ . When the Ni content is 0 wt.%, the ceramic particles show severe sintering, and a large number of obvious holes can be observed in the low magnification photos. When the Ni content increases from 10 wt.% to 50 wt.%, the ceramic particle size gradually decreases from  $\sim 5$   $\mu\text{m}$  to  $\sim 0.5$   $\mu\text{m}$ . The main reasons for the decrease in ceramic particle size may be as follows: (1) the crystal growth is an exponential function of temperature [20]. With the increase in Ni content, the combustion temperature gradually decreases, and the growth rate of  $\text{ZrB}_2$  and  $\text{ZrC}$  decreases; (2) with the increase in Ni content, the thermal conductivity of the product increases, making the cooling rate increase, which is not conducive to the growth of ceramic particles [21]; and (3) with the increase in Ni content, the liquid phase between the ceramic particles increases during the reaction process, which hinders the sintering growth between the grains and reduces the trend of grain coarsening.

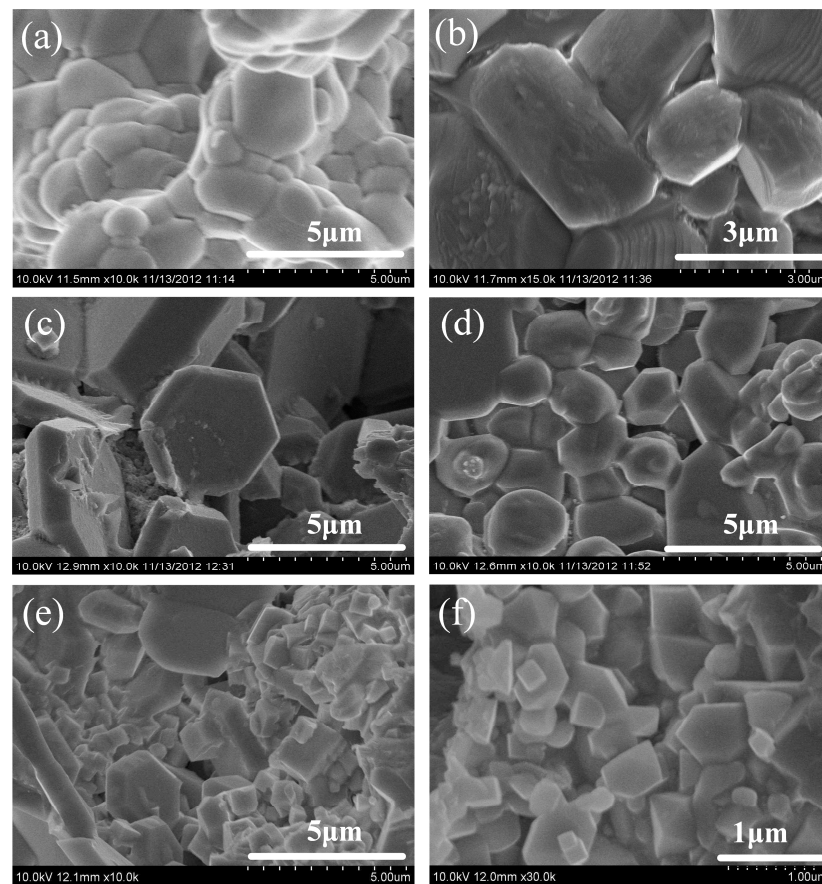


**Figure 7.** Microstructures of the SHS products with the reactant Ni contents of (a) 0 wt.%, (b) 10 wt.%, (c) 20 wt.%, (d) 30 wt.%, (e) 40 wt.%, and (f) 50 wt.%.

### 3.1.2. Effect of $B_4C$ Particle Sizes on the SHS Reaction

The 30 wt.% Ni-Zr- $B_4C$  system was used as the research object. In the reaction mixture, the particle size of  $B_4C$  was 3.5  $\mu m$ , 14  $\mu m$ , 28  $\mu m$ , 40  $\mu m$ , and 80  $\mu m$ , the particle size of Ni was 48  $\mu m$ , and the particle size of Zr was 38  $\mu m$ .

The products after the reaction of the samples with different  $B_4C$  powder were analyzed by XRD, as illustrated in Figure 8. When the particle size of the  $B_4C$  powder in the reactants is 3.5  $\mu m$ , 14  $\mu m$ , and 28  $\mu m$ , the SHS products were composed of  $ZrB_2$ ,  $ZrC$ , Ni, and a small amount of intermediate  $Ni_2B$ . With the increase in the particle size of the  $B_4C$  powder, the ignition delay time of the SHS reaction increased. When the  $B_4C$  size in the reactant was larger than 40  $\mu m$ , the self-propagating reaction became very difficult, and the ignition time was longer. The product contained large amounts of  $NiZr$ ,  $Ni_{10}Zr_7$ , and  $Ni_2B$ , but the amounts of  $ZrB_2$  and  $ZrC$  were very small. When the particle size of the  $B_4C$  powder in the reactant was 80  $\mu m$ , the reaction could not be self-propagated, and almost no  $ZrB_2$  and  $ZrC$  were generated. The above results show that the SHS reaction behavior and the products of the 30 wt.% Ni-Zr- $B_4C$  system were significantly affected by the size of the  $B_4C$  particles. The increase in the  $B_4C$  particle size makes the ignition and propagation process of the self-propagating reaction difficult, and also reduces the propagation rate of the combustion wave and the product formation rate. A similar effect was found in the Cu-Zr- $B_4C$  system, in which coarser  $B_4C$  particles postponed the formation of  $ZrB_2$  and  $ZrC$  [5]. The results show that the dissolution rate of  $B_4C$  in Cu-Zr liquid decreased with the increase in  $B_4C$  size, which could retard the formation of the Cu-Zr-B-C liquid. This led to the incomplete conversion of  $ZrB_2$  and  $ZrC$ .

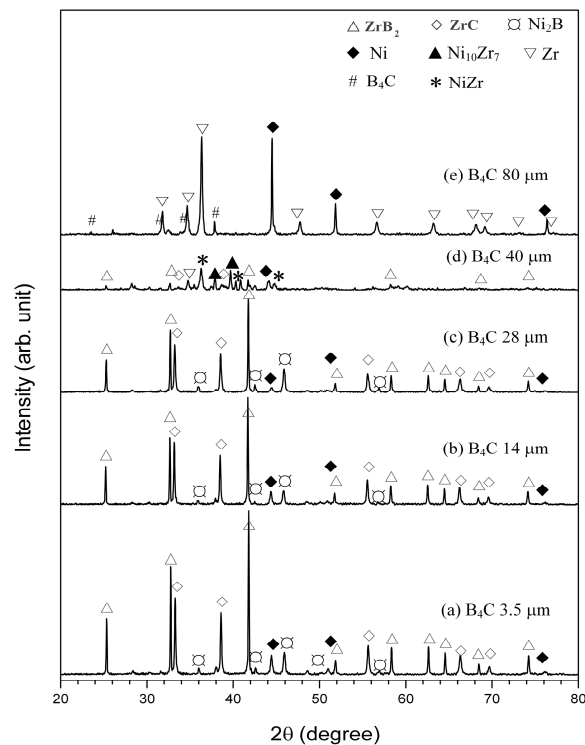


**Figure 8.** XRD patterns for SHS products of the 30 wt.% Ni-Zr-B<sub>4</sub>C system with various B<sub>4</sub>C particle sizes: (a) 3.5 μm, (b) 14 μm, (c) 28 μm, (d) 40 μm, and (e) 80 μm.

### 3.2. Formation Mechanism of ZrB<sub>2</sub> and ZrC during the SHS Process

#### 3.2.1. DSC Analysis

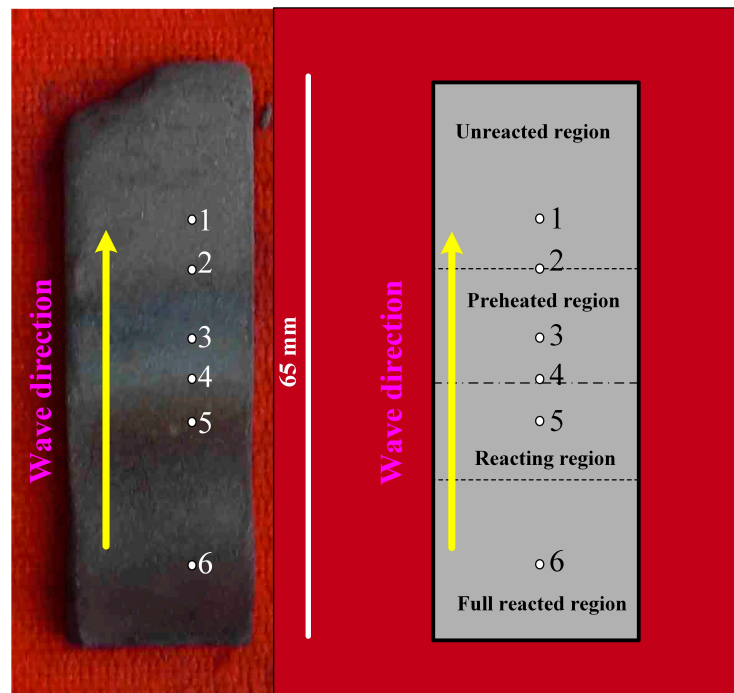
The reaction mechanism of the 30 wt.% Ni-Zr-B<sub>4</sub>C system during the DSC experiment was described in detail in a previous paper [14]. It was proposed as follows: firstly, Ni, B<sub>4</sub>C, and Zr have solid-state diffusion reactions to form some Ni<sub>x</sub>Zr<sub>y</sub> and Ni<sub>x</sub>B<sub>y</sub> intermetallics. Then, an Ni-B eutectic liquid formed at about 1025 °C, and the free C atoms dissolved into the Ni-B liquid to form an Ni-B-C ternary liquid. When the mixture was heated to about 1088 °C, part of Zr powder directly reacted with B<sub>4</sub>C through solid-state diffusion reaction, and part of the Zr powder dissolved into the Ni-B-C ternary liquid to form the Ni-Zr-B-C quaternary liquid. When the temperature reached 1150 °C, an Ni-Zr eutectic liquid formed. The Ni-Zr eutectic liquid could also dissolve into the Ni-B liquid or Ni-B-C liquid to form Ni-Zr-B-C quaternary liquid. Finally, ZrB<sub>2</sub> and ZrC precipitated out of the saturated liquid.

#### 3.2.2. Combustion Wave Quenching Experiment

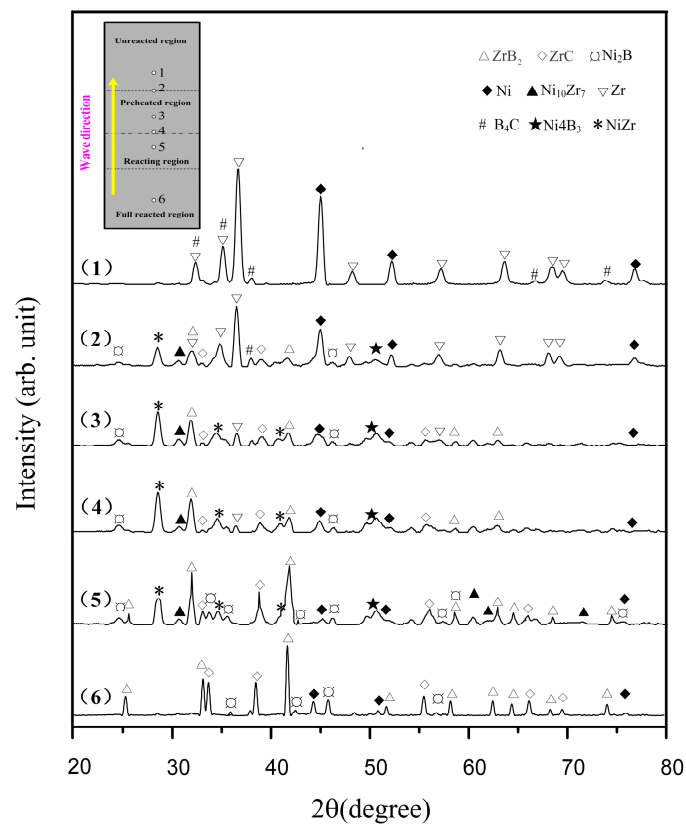
Although the above DSC analysis result is very helpful to understand the formation mechanism of the Ni-Zr-B<sub>4</sub>C system, the DSC experimental condition is different from the SHS in the glove box in terms of heating rate, sample volume, and compacting rate. These factors have a great influence on the reaction kinetics and mechanism of the system. Therefore, the reaction mechanism under the DSC condition cannot be used to fully explain the reaction mechanism under the SHS mode. In order to study the reaction mechanism of the ZrB<sub>2</sub> and ZrC of the Ni-Zr-B<sub>4</sub>C system formed by the SHS in glove box, a combustion wave quenching experiment was conducted. The quenched sample was analyzed by XRD and SEM, and the reaction mechanism was studied.

Figure 9 shows the macroscopic morphology and partition diagram of the SHS quenched bar, in which the wavy area with the darkest color is the typical morphology of the combustion wave. Against the spreading direction of combustion wave, the quenched bar can be differentiated into four regions according to the degree of reaction, namely, the unreacted region, the preheated region, the reacting region, and the fully reacted region. As shown in Figure 9, six points are noted in each reaction region and the interface between

the two regions, respectively. Figure 10 shows the X-ray micro-diffraction patterns for each point.



**Figure 9.** Macroscopic morphology and partition diagram showing different regions of the SHS quenched bar.



**Figure 10.** X-ray micro-diffraction patterns in different regions of the SHS quenched bar: (1) unreacted region, (2) preheated region, (3–5) reacting region, and (6) fully reacted region, respectively.

Figure 11 shows the microstructure of the Ni, Zr, B<sub>4</sub>C raw material powder and the unreacted region of the quenched bar. It is observed that the Ni, Zr, and B<sub>4</sub>C powders can be easily distinguished from the morphology. Among them, the Ni particles show clusters of flowers, the Zr particles show smooth clumps, and the B<sub>4</sub>C particles show irregular shapes with sharp corners (see Figure 11a–c). In addition, the distribution of the reactants in the unreacted region is relatively uniform (see Figure 11d). The interface between the unreacted region and the preheated region and the typical morphology of the preheated region are presented in Figure 12a,b, respectively. It can be observed from Figure 12a that the morphology of the unreacted region is obviously different from that of the preheated region. The unreacted region is composed of a loose reactant powder mixture, while the preheated region is relatively dense, and there is an interface region between them. The change from point (2) to point (3) in the XRD results is shown in Figure 10, indicating that Ni reacted with Zr in the preheated region, forming NiZr, with a high content. Meanwhile, the formation of Ni<sub>2</sub>B and Ni<sub>4</sub>B<sub>3</sub> indicated that a solid diffusion reaction also occurred between Ni and B<sub>4</sub>C. With the increase in temperature, Ni<sub>2</sub>B and Ni<sub>4</sub>B<sub>3</sub> could form the Ni-B liquid phase when they reached the eutectic point (1291 K) [22], which rapidly spread out and filled into the pores of the sample, thus forming a relatively dense structure, as shown in Figure 12b.

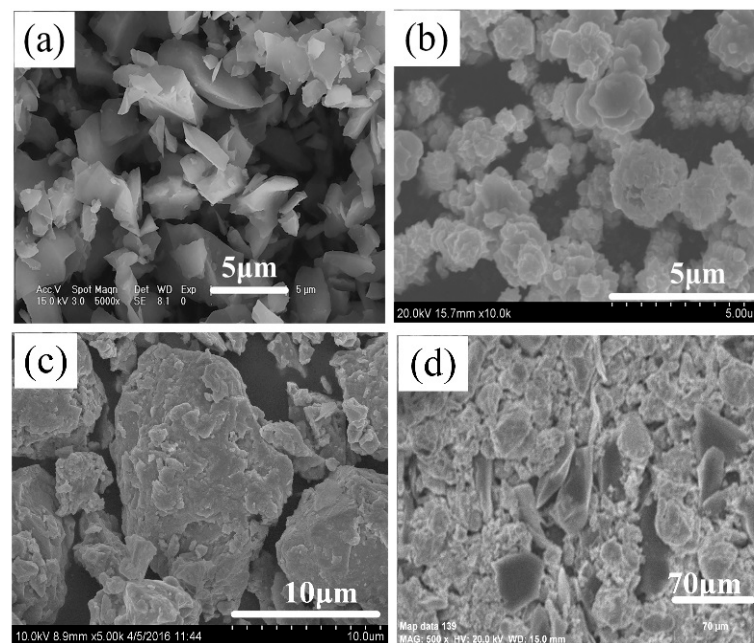


**Figure 11.** Microstructure of (a) Ni, (b) Zr, (c) B<sub>4</sub>C raw material powder, and (d) the unreacted region of the quenched bar.

It is worth mentioned that some papers [22] stated that TiC, rather than TiB<sub>2</sub>, would preferentially form in the metal-Ti-B<sub>4</sub>C system. However, the outcomes of this work are different, and there is no preferential formation of ZrC in the preheated region because the eutectic temperature of Ni<sub>x</sub>Zr<sub>y</sub> is much larger than that of the reported Ni<sub>x</sub>Ti<sub>y</sub>.

Figure 12c exhibits the typical morphology of the reacting region. This region was more compact than the preheated region due to more liquid phase filling. It could also be observed that B<sub>4</sub>C was tightly surrounded by the liquid phase, and a portion of B<sub>4</sub>C had reacted. According to X-ray micro-diffraction and previous DSC results, the reaction between Zr and B<sub>4</sub>C occurred first in this region, and a great quantity of exothermic heat was released. The temperature of the system increased to reach the eutectic temperature of Ni<sub>10</sub>Zr<sub>7</sub>-Ni (1423 K) and NiZr-Ni (1443 K) [23], and the Ni-Zr liquid phase was formed. The quaternary Ni-Zr-B-C liquid phase was formed after dissolving with the Ni-B liquid phase

and dissolving some C atoms; then, a great quantity of  $ZrB_2$  and  $ZrC$  were precipitated from the liquid phase.

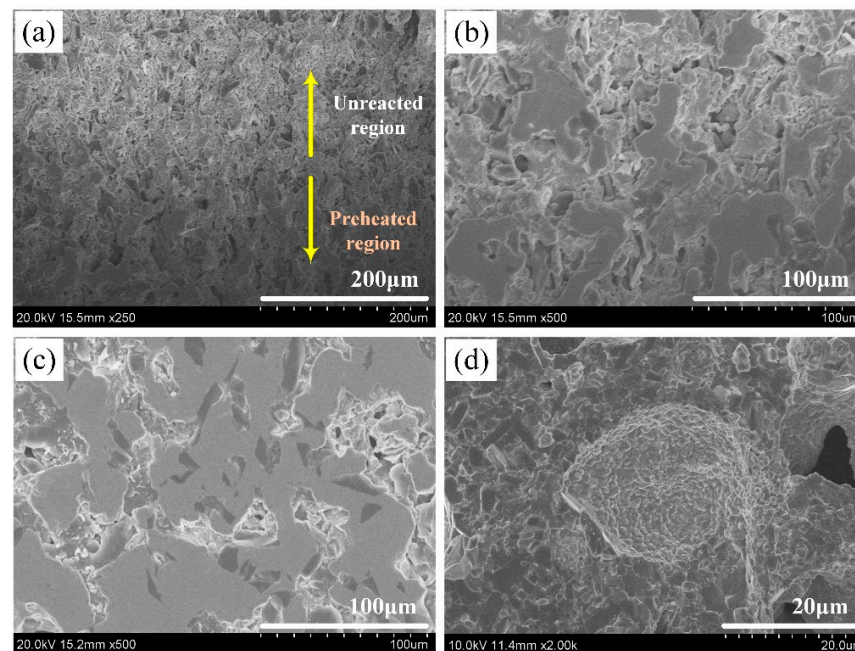


**Figure 12.** Microstructure of the (a) interface between the unreacted region and the preheated region, (b) preheated region, (c) reacting region, (d) fully reacted region, respectively.

Figure 13 shows the morphology around the  $B_4C$  particles in the reacting region and the EDS-line analysis of each element. The left part of the figure shows the interface between Zr and  $B_4C$ , and a high content of the Zr element was also detected near the interior of  $B_4C$ , indicating that a solid–solid reaction between Zr and  $B_4C$  occurred, and a portion of  $ZrB_2$  and  $ZrC$  were formed through this reaction. The right part of the figure shows the interface between the Ni-Zr liquid phase and  $B_4C$ , where parts B and C could obviously diffuse into the Ni-Zr liquid phase.

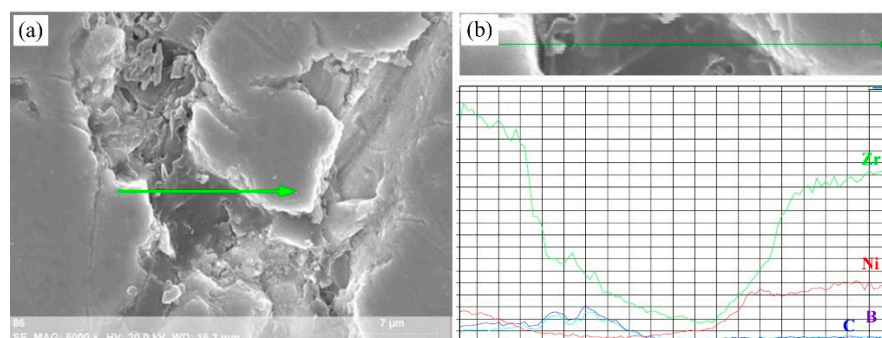


**Figure 13.** Microstructure of a remnant  $B_4C$  particle dissolving into the Ni-Zr-B-C melt and the corresponding EDS-line analysis in the combustion region: (a) SEM image and (b) EDS-line analysis.

The microstructure of the fully reacted region is illustrated in Figure 12d. With the formation and saturation of a great quantity of the Ni-Zr-B-C liquid phase, a large amount of  $ZrB_2$  and  $ZrC$  was precipitated. It can be seen that the  $B_4C$  particles were decomposed, and some holes were left at the original positions of the  $B_4C$  particles.

Therefore, the reaction mechanism in the Ni-Zr- $B_4C$  system during SHS is proposed as follows: (1)  $Ni + Zr + B_4C \rightarrow$  (2)  $NiZr + Ni_{10}Zr_7 + Ni_2B + Ni_4B_3 + Ni + Zr + B_4C \rightarrow$  (3)

$\text{NiZr} + \text{Ni}_{10}\text{Zr}_7 + \text{Ni-B (liquid)} + \text{ZrB}_2 + \text{ZrC} \rightarrow (4) \text{Ni-Zr (liquid)} + \text{Ni-B (liquid)}$  or  $\text{Ni-B-C (liquid)} + \text{ZrB}_2 + \text{ZrC} \rightarrow (5) \text{Ni-Zr-B-C (liquid)} + \text{ZrB}_2 + \text{ZrC} \rightarrow (6) \text{ZrB}_2 + \text{ZrC} + \text{Ni}$ .

Based on the results of the DSC analysis and quenching experiment, it was determined that the reaction mechanism of  $\text{ZrB}_2$  and  $\text{ZrC}$  under the two conditions was basically the same. Initially, Ni reacted with  $\text{B}_4\text{C}$  and Zr to form  $\text{Ni}_2\text{B}$ ,  $\text{Ni}_4\text{B}_3$ ,  $\text{NiZr}$ ,  $\text{Ni}_{10}\text{Zr}_7$ , and other intermediate phases. As the temperature increased,  $\text{Ni}_2\text{B}$  and  $\text{Ni}_4\text{B}_3$  formed an Ni-B eutectic liquid phase. When the temperature increased further, some Zr directly reacted with  $\text{B}_4\text{C}$ , and a large amount of heat was released to promote the temperature increase in the system. After reaching the eutectic temperature of  $\text{Ni}_{10}\text{Zr}_7$ ,  $\text{NiZr}$ , and Ni, an Ni-Zr binary liquid phase was formed. When the two binary liquids mixed with each other, and some free C dissolved into it, the Ni-Zr-B-C quaternary liquid phase was formed. Finally, when the concentration of [Zr], [B], and [C] in the liquid met the conditions for the formation of  $\text{ZrB}_2$  and  $\text{ZrC}$ , a large amount of  $\text{ZrB}_2$  and  $\text{ZrC}$  precipitated out of the saturated liquid.

The difference is that under the DSC condition, the reactant system showed a loose morphology, a small heating rate, and a large heat loss, leading to a slow liquid phase formation rate, and a long reaction time to precipitate  $\text{ZrB}_2$  and  $\text{ZrC}$  from the liquid phase. In the SHS reaction, the reactant had a high heating rate and a small heat loss, which can quickly form the liquid phase and instantly generate a large amount of  $\text{ZrB}_2$  and  $\text{ZrC}$ .

#### 4. Conclusions

$\text{ZrB}_2$ - $\text{ZrC}$ /Ni cermets were successfully synthesized by SHS using the Ni-Zr- $\text{B}_4\text{C}$  system. The SHS reaction behavior and the formation mechanism of ceramic particles were systematically studied.

(1) With the increase in Ni content, the adiabatic temperature ( $T_{\text{ad}}$ ), the maximum combustion temperature ( $T_c$ ), the ignition delay time ( $t_{\text{ig}}$ ), and the ceramic particle size in the product all showed a gradually decreasing trend. When the content of Ni was low, the product was mainly composed of Ni,  $\text{ZrB}_2$ , and  $\text{ZrC}$ . When the content of Ni exceeded 40 wt.%, a large number of the intermediate phases existed in the product.

(2) With the increase in  $\text{B}_4\text{C}$  powder size, the ignition and propagating process of the SHS reaction became more and more difficult, and the spread rate of combustion wave and the formation rate of product gradually decreased. When the particle size of the  $\text{B}_4\text{C}$  powder was larger than 40  $\mu\text{m}$ , the product contained a large number of intermediate phases.

(3) It is revealed that the formation mechanism of  $\text{ZrB}_2$  and  $\text{ZrC}$  in the Ni-Zr- $\text{B}_4\text{C}$  system under the DSC condition and the SHS reaction in the glove box is basically the same. Initially, Ni reacted with  $\text{B}_4\text{C}$  and Zr to form some intermediates such as  $\text{Ni}_2\text{B}$ ,  $\text{Ni}_4\text{B}_3$ ,  $\text{NiZr}$ , and  $\text{Ni}_{10}\text{Zr}_7$ , and then the Ni-B eutectic liquid phase formed. As a part of Zr directly reacted with  $\text{B}_4\text{C}$ , a great quantity of heat was released to promote the increase in the system temperature, and the Ni-Zr binary liquid phase formed. When the two binary liquids mixed with each other and some free C dissolved into it, the Ni-Zr-B-C quaternary liquid phase formed. Finally, a great quantity of  $\text{ZrB}_2$  and  $\text{ZrC}$  were precipitated out of the saturated liquid. These results are expected to provide a theoretical basis for the formation mechanism of  $\text{ZrB}_2$ - $\text{ZrC}$ /metal cermet composites using the SHS method.

**Author Contributions:** All authors contributed to the study design, data analysis, and discussion, as well as to the writing and editing of the manuscript. Study conception and design: J.X. and B.Z.; experimental work: J.X. and P.M.; data analysis: J.X.; manuscript writing and editing: J.X., P.M. and X.Y. All authors have read and agreed to the published version of the manuscript.

**Funding:** This research was supported by the National Natural Science Foundation of China (Grant No. 11904126), the Scientific Research Fund of Jilin Provincial Education Department, China (Grant No. JJKH20200250KJ, JJKH20220232KJ), and the Natural Science Foundation of Jilin Province (Grant No. YDZJ202201ZYTS429).

**Data Availability Statement:** Not applicable.

**Conflicts of Interest:** The authors declare no conflict of interest.

## References

1. Hu, Q.D.; Luo, P.; Zhang, M.X.; Song, M.S.; Li, J.G. Combustion and formation behavior of hybrid ZrB<sub>2</sub> and ZrC particles in Al-Zr-B<sub>4</sub>C system during self-propagation high temperature synthesis. *Int. J. Refract. Met. Hard Mater.* **2012**, *31*, 89–95. [[CrossRef](#)]
2. Zhang, M.X.; Huo, Y.Q.; Huang, M.; Fang, Y.H.; Zou, B.L. In situ synthesis and formation mechanism of ZrC and ZrB<sub>2</sub> by combustion synthesis from the Co-Zr-B<sub>4</sub>C system. *J. Asian Ceram. Soc.* **2015**, *3*, 271–278. [[CrossRef](#)]
3. Zhang, M.X.; Zou, B.L.; Xu, J.Y.; Cai, X.L.; Wang, Y.; Huang, M.; Fang, Y.H.; Huo, Y.Q.; Cao, X.Q. Reaction behavior, microstructure and application in coating of in situ ZrC-ZrB<sub>2</sub> ceramic composites powders from a Co-Zr-B<sub>4</sub>C system. *Mater. Des.* **2015**, *81*, 65–72. [[CrossRef](#)]
4. Zhang, M.X.; Huo, Y.Q.; Hu, Q.D.; Zhang, P.; Zou, B.L. Reaction behavior and formation mechanism of ZrC and ZrB<sub>2</sub> in the Cu-Zr-B<sub>4</sub>C system. *Int. J. Refract. Met. Hard Mater.* **2014**, *43*, 102–108. [[CrossRef](#)]
5. Zhang, M.X.; Huo, Y.Q.; Huang, M.; Fang, Y.H.; Wang, G.P. The effect of B<sub>4</sub>C particle size on the reaction process and product in the Cu-Zr-B<sub>4</sub>C system. *J. Asian Ceram. Soc.* **2015**, *3*, 38–43. [[CrossRef](#)]
6. Zhu, G.L.; Wang, W.; Wang, R.; Zhao, C.B.; Pan, W.T.; Huang, H.J.; Du, D.F.; Wang, D.H.; Shu, D.; Dong, A.P.; et al. Formation mechanism of spherical TiC in Ni-Ti-C system during combustion synthesis. *Materials* **2017**, *10*, 1007. [[CrossRef](#)] [[PubMed](#)]
7. Liang, Y.H.; Wang, H.Y.; Yang, Y.F.; Du, Y.L.; Jiang, Q.C. Reaction path of the synthesis of TiC-TiB<sub>2</sub> in Cu-Ti-B<sub>4</sub>C system. *Int. J. Refract. Met. Hard Mater.* **2008**, *26*, 383–388. [[CrossRef](#)]
8. Zou, B.L.; Xu, J.Y.; Wang, Y.; Zhao, S.M.; Fan, X.Z.; Hui, Y.; Zhou, X.; Huang, W.Z.; Cai, X.L.; Tao, S.Y.; et al. Self-propagating high-temperature synthesis of TiC-TiB<sub>2</sub>-based Co cermets from a Co-Ti-B<sub>4</sub>C system and fabrication of coatings using the cermet powders. *Chem. Eng. J.* **2013**, *233*, 138–148. [[CrossRef](#)]
9. Yang, Y.F.; Wang, H.Y.; Zhao, R.Y.; Liang, Y.H.; Jiang, Q.C. Effect of Ni content on the reaction behaviors of self-propagating high-temperature synthesis in the Ni-Ti-B<sub>4</sub>C system. *Int. J. Refract. Met. Hard Mater.* **2008**, *26*, 77–83. [[CrossRef](#)]
10. Levashov, E.A.; Mukasyan, A.S.; Rogachev, A.S.; Shtansky, D.V. Self-propagating high-temperature synthesis of advanced materials and coatings. *Int. Mater. Rev.* **2017**, *62*, 203–239. [[CrossRef](#)]
11. Jin, S.B.; Su, H.K.; Sha, G. Atom Probe tomography analysis of TiC<sub>x</sub> powders synthesized by SHS in Al/Fe/Cu-Ti-C systems. *Materials* **2019**, *12*, 4095. [[CrossRef](#)] [[PubMed](#)]
12. Matveev, A.E.; Promakhov, V.; Nikitin, P.; Babaev, A.; Vorozhtsov, A. Effect of mechanical activation of Al-Ti-B powder mixture on phase composition and structure of Al-TiB<sub>2</sub> composite materials obtained by self-propagating high-temperature synthesis (SHS). *Materials* **2022**, *12*, 2668. [[CrossRef](#)] [[PubMed](#)]
13. Xu, J.Y.; Zou, B.L.; Zhao, S.M.; Hui, Y.; Huang, W.Z.; Zhou, X.; Wang, Y.; Cai, X.L.; Cao, X.Q. Fabrication and properties of ZrC-ZrB<sub>2</sub>/Ni cermet coatings on a magnesium alloy by atmospheric plasma spraying of SHS powders. *Ceram. Int.* **2014**, *40*, 15537–15544. [[CrossRef](#)]
14. Xu, J.Y.; Ma, P.F.; Zou, B.L. Reaction mechanism of ZrB<sub>2</sub>-ZrC formation in Ni-Zr-B<sub>4</sub>C system analyzed by differential scanning calorimetry. *Materials* **2021**, *14*, 6467. [[CrossRef](#)]
15. Moore, J.J.; Feng, H.J. Combustion synthesis of advanced materials: Part I: Reaction parameters. *Prog. Mater. Sci.* **1995**, *39*, 243–273. [[CrossRef](#)]
16. Barin, I. *Thermochemical Data of Pure Substances*, 3rd ed.; Wiley-VCH Verlag GmbH: Weinheim, Germany, 1995.
17. Zou, B.L.; Shen, P.; Jiang, Q.C. Dependence of the SHS reaction behavior and product on B<sub>4</sub>C particle size in Al-Ti-B<sub>4</sub>C and Al-TiO<sub>2</sub>-B<sub>4</sub>C systems. *Mater. Res. Bull.* **2009**, *44*, 499–504. [[CrossRef](#)]
18. Matveev, A.E.; Nikitin, P.Y.; Zhukov, I.A.; Zhukov, A.S. The use of plastic waste as carbon raw materials to obtain TiC-based powders. *Ceram. Int.* **2021**, *47*, 21140–21146. [[CrossRef](#)]
19. Nikitin, P.Y.; Zhukov, I.A.; Matveev, A.E.; Sokolov, S.D.; Boldin, M.S.; Vorozhtsov, A.B. AlMgB<sub>14</sub>-TiB<sub>2</sub> composite materials obtained by self-propagating high-temperature synthesis and spark plasma sintering. *Ceram. Int.* **2020**, *46*, 22733–22737. [[CrossRef](#)]
20. Choi, Y.; Rhee, S.W. Effect of aluminum addition on the combustion reaction of titanium and carbon to form TiC. *J. Mater. Sci.* **1993**, *28*, 6669–6675. [[CrossRef](#)]
21. Yang, Y.F.; Wang, H.Y.; Zhao, R.Y.; Jiang, Q.C. Effect of reactant particle size on the self-propagating high-temperature synthesis reaction behaviors in the Ni-Ti-B<sub>4</sub>C system. *Metall. Mater. Trans. A* **2009**, *40*, 232–239. [[CrossRef](#)]
22. Massalski, T.B.; Okamoto, H.; Subramanian, P.R. *Binary Alloy Phase Diagrams*, 2nd ed.; ASM International: Metals Park, OH, USA, 1990.
23. Hayes, E.T.; Roberson, A.H.; Paasche, O.G. The Zirconium-Nickel phase diagram. *Trans. ASM* **1953**, *45*, 893–900.

**Disclaimer/Publisher's Note:** The statements, opinions and data contained in all publications are solely those of the individual author(s) and contributor(s) and not of MDPI and/or the editor(s). MDPI and/or the editor(s) disclaim responsibility for any injury to people or property resulting from any ideas, methods, instructions or products referred to in the content.